Sediment formation by Brownian dynamics simulation: Effect of colloidal and hydrodynamic interactions on the sediment structure

Geoffrey C. Ansell and Eric Dickinson

Citation: The Journal of Chemical Physics **85**, 4079 (1986); doi: 10.1063/1.450879
View online: http://dx.doi.org/10.1063/1.450879
View Table of Contents: http://scitation.aip.org/content/aip/journal/jcp/85/7?ver=pdfcov
Published by the AIP Publishing

Sediment formation by Brownian dynamics simulation: Effect of colloidal and hydrodynamic interactions on the sediment structure

Geoffrey C. Ansell and Eric Dickinson[a)]
Procter Department of Food Science, University of Leeds, Leeds LS2 9JT, England

(Received 7 May 1986; accepted 27 June 1986)

The formation of a gel-like sediment by a process of irreversible single-particle accretion has been simulated in three dimensions by the computational technique of Brownian dynamics. The model incorporates hydrodynamic interactions between spherical particles at the level of the Rotne–Prager approximation, and colloidal interactions are described in terms of the Derjaguin–Landau–Verwey–Overbeek (DLVO) pair potential of mean force for electrostatically stabilized particles. The density and structure of simulated sediments have been determined as a function of ionic strength and sedimenting field strength. Depending on the conditions, sediment volume fractions range from 0.09 to 0.33. Colloidal forces can significantly affect the short-range structure of low-density diffusion-controlled sediments. Sediment density increases strongly with increasing field strength, and sediment structures as measured by the particle pair distribution function become more liquid-like as the volume fraction increases. Hydrodynamic interactions have little effect on aggregate structure at low field strengths where Brownian aggregation is dominant, but the presence of hydrodynamic interactions is essential for the formation of high-density sediments at high field strengths. This work suggests that, in general, colloidal forces and hydrodynamic interactions cannot be neglected in simulations of colloidal aggregration and gelation.

I. INTRODUCTION

One of the principal objectives of colloid science is to understand the structure and properties of dispersions, aggregates, and gels in terms of the microscopic interactions between the constituent colloidal particles. Recently, there has developed renewed interest in the theory of colloidal aggregation following the demonstration of Witten and Sander[1] that a simple random growth model can give the essential self-similar features of diffusion-limited aggregation. The Witten–Sander model is important also because structures generated by it have interesting scaling and universality properties whose implications extend over a wide range of physical processes.[2] Studies of the growth of fractal-type aggregates using various computer simulation models has been the main stimulus to recent progress in this field, given the formidable practical difficulties associated with the experimental determination of colloidal aggregate structure.[3–6] Computer simulation enables the different factors affecting aggregate structure and growth to be investigated systematically and independently. In this paper we are interested in the effect of ionic strength and hydrodynamic interactions on the structure of aggregates formed by sedimentation in a dilute dispersion of spherical particles interacting with colloidal potentials of the Derjaguin–Landau–Verwey–Overbeek (DLVO) form. To simulate the particle motion in real time, we use the technique of Brownian dynamics with hydrodynamic interactions.[7]

In earlier work on the simulation of colloid coagulation in nondilute systems, we have studied the very initial stages of the process in three dimensions[8] and have presented preliminary results for realistic cluster–cluster (ClCl) aggregation in two dimensions.[9] In the two-dimensional study of nonhydrodynamically interacting DLVO-type particles, we found[9] that the nature of the colloidal forces has little effect on the long-range aggregate structure as measured by the scaling of the radius of gyration, but has considerable influence on the short-range aggregate structure as measured by the particle–particle pair distribution function. However, the inclusion of realistic interparticle interactions, and the computational complexity of simulating the Brownian dynamics of aggregates using a constraints algorithm,[10] puts limitations on the size of systems that can be studied, as compared, for instance, with the simpler lattice models of Meakin[11] and others.[2] In the present paper, we look at the structure of sediments formed by *single*-particle deposition, which enables us to dispense with the problem of enforcing constraints, and to include hydrodynamic interactions in an approximate but reasonably realistic way. The problem studied here is of considerable practical importance in relation to such processes as soiling and filtration.

Using simple lattice models, Meakin has investigated[11] how the structure of sediments deposited in two and three dimensions are affected by the sticking probability and the type of particle trajectory. He found that a low sticking probability gives structures which are more dense than those generated with a high sticking probability, and that ballistic trajectories give more dense sediments than Brownian trajectories. For single-particle and ClCl deposition, the scaling properties have been investigated in some detail.[12,13] From the experimental viewpoint, probably the most realistic treatment of deposition so far reported is that of Voss and Tomkiewicz.[14] In this lattice treatment of electrodeposition, the effects of ClCl aggregation, concentration gradients, and sticking probability were each related to experimental vari-

[a)] To whom all correspondence should be addressed.

 0021-9606/86/194079-08$02.10

ables in electrolysis (e.g., sticking probability was related to electrical overpotential). In this way, Voss and Tomkiewicz were able to compare their simulation results with experiment, and they found that the model correctly predicted the existence of a critical overpotential and an initialization time, as well as generating deposits which, qualitatively at least, were of the same morphology as those found experimentally.

Lattice models give valuable insight into underlying scaling behavior, but they cannot describe the close-range spatial structure in aggregates or gels formed from spherical particles in an electrostatically or polymerically stabilized colloidal system. Little is known quantitatively about the relationship betwen the nature of colloidal forces during aggregation and the statistical arrangement of particles in the aggregated structure. Intuitively, one would expect the inclusion of hydrodynamic interactions to lead to denser sediments, with particles slipping past one another rather than bumping directly into one another. Also, one would expect the presence of a potential energy barrier to coagulation to affect the aggregation in a manner analogous to a low sticking probability. In this paper we study the effect of these particle interactions on sediment density and structure using a nonlattice simulation model. The simulation methodology and the assumed forms of particle interactions are described in Sec. II. Computational details of the sedimentation model are set out in Sec. III. Results and discussion are presented in Sec. IV for sediments generated under different conditions of ionic strength and sedimenting field strength. Finally, the conclusions to be drawn are given in Sec. V.

II. BROWNIAN DYNAMICS

In simulating a system of solute particles and solvent molecules, where one is interested only in the dynamics of the solute particles, it is convenient to use a stochastic dynamics approach in preference to the more conventional molecular dynamics approach used in connection with simple liquids. Stochastic dynamics based on the Langevin equation of motion was introduced into chemical physics by Turq *et al.*[15] in 1977, and since then in a variety of extended forms it has been applied to many types of dynamical phenomena.[16–18] When the particles are of colloidal size, inertial terms and time correlations can usually be neglected, and the technique is called Brownian dynamics. The movement of colloidal particles in a Brownian dynamics simulation is diffusive in nature, with spatial correlations in the motion determined by hydrodynamic interactions between the particles.

The Brownian dynamics algorithm used here was introduced by Ermak and McCammon.[19] For a system of N particles, the moving-on routine can be written in the form

$$\mathbf{x}_i = \mathbf{x}_i^\circ + \sum_j \left(\frac{\partial \mathsf{D}_{ij}^\circ}{\partial \mathbf{x}_j}\right)\Delta t + (\Delta t/kT)\sum_j \mathsf{D}_{ij}^\circ \mathbf{F}_j^\circ + \mathbf{R}_i(\mathsf{D}_{ij}^\circ, \Delta t), \quad (i,j = 1,N), \qquad (1)$$

where $\mathbf{x}_i$ is the coordinate vector of particle i, D_{ij} is the diffusion tensor for particles i and j, $\mathbf{F}_j$ denotes the nonhydrodynamic force associated with particle j, k is Boltzmann's constant, T is the absolute temperature, and Δt is the timestep between successive iterations. The superscript $^\circ$ refers to quantities calculated at the beginning of the timestep. The stochastic term $\mathbf{R}_i$ has first and second probability moments

$$\langle \mathbf{R}_i(\Delta t)\rangle = 0,$$
$$\langle \mathbf{R}_i(\Delta t)\mathbf{R}_j(\Delta t)\rangle = 2\mathsf{D}_{ij}^\circ \Delta t. \qquad (2)$$

It is assumed that the timestep is sufficiently short that $\mathbf{F}_j$ and D_{ij} remain essentially constant during the interval Δt. We are not concerned here with rotational Brownian motion, although it can be included in a more generalized scheme in simulations where orientational correlations are important.[20]

Hydrodynamic interactions are included in the simulation through the diffusion tensor D_{ij}. For spherical particles of radius a with center-to-center separation r, expressions are available[21–23] for D_{ij} as a series in powers of (a/r), and many-body effects can also be included.[24] In practice, however, these analytical expressions are too unwieldy to be used in large-scale simulations, and so here we approximate hydrodynamic interactions by the Rotne–Prager tensor[25]

$$\mathsf{D}_{ij} = D_0[\delta_{ij}1 + (3a/4r)(\hat{\mathbf{r}}_{ij}\hat{\mathbf{r}}_{ij} + 1) - (3/2)(a/r)^3(\hat{\mathbf{r}}_{ij}\hat{\mathbf{r}}_{ij} - \tfrac{1}{3}1)]. \qquad (3)$$

In Eq. (3), $\hat{\mathbf{r}}_{ij}$ is the unit vector between particles i and j, and D_0 is the Stokes diffusion coefficient. The Rotne–Prager tensor (modified Oseen tensor) has been used successfully to describe the hydrodynamic properties of macromolecules in terms of assemblies of connected spherical subunits.[26] From the simulation viewpoint, it has the advantage of being simple but well-behaved. The tensor is divergenceless, thereby allowing the gradient term to be dropped from Eq. (1). In multiparticle systems it always gives a positive-definite $3N \times 3N$ diffusion matrix, unlike the simple Oseen tensor which has the serious computational disadvantage of giving imaginary stochastic weightings in some regions of configurational phase space.[8] The Rotne–Prager tensor only becomes invalid when particle surfaces get very close.[27] For the colloidal potentials assumed here (see below), when a pair of particles is held in the secondary minimum, the trace of the two-body matrix is overestimated by $\sim 10\%$ as compared with the exact hydrodynamic expressions.[21]

The quantities $\{\mathbf{F}_j\}$ in Eq. (1) contain contributions from both the sedimenting forces acting just in the z direction and the interparticle colloidal forces acting in x, y, and z directions. Particles are assumed to interact with pair potentials of mean force $U(r)$ of the Derjaguin–Landau–Verwey–Overbeek (DLVO) form[28]:

$$U(r) = U_R(r) + U_A(r), \qquad (4)$$

where $U_R(r)$ is the screened Coulombic repulsion and $U_A(r)$ is the van der Waals attraction. Under conditions where DLVO potentials are pairwise-additive ($\kappa a \gg 1$), $U(r)$ is given by[28]

$$U(r) = 2\pi\epsilon_r\epsilon_0 a\psi_0^2 \ln[1 + \exp(-\kappa s)], \qquad (5)$$

where ϵ_r is the relative dielectric constant of the medium, ϵ_0 is the permittivity of free space, ψ_0 is the particle surface potential, $s = r - 2a$ is the surface-to-surface separation,

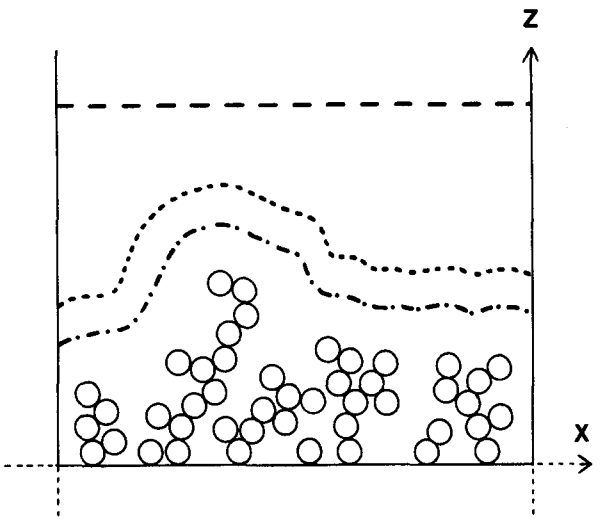

FIG. 1. Schematic representation of simulation reaction box. The unit cell has a solid square base of dimensions $40a \times 40a$ where a is the particle radius. The cell is open at the top and periodic in the x and y directions (particles diffusing through the left-hand wall reemerge through the right-hand wall, and *vice versa*). In a Brownian dynamics run, single particles are successively introduced with random x and y coordinates at a distance $15a$ above the highest point on the growing sediment (– – –). The lines (---) and (– · –) denote when Brownian motion/hydrodynamics and DLVO interactions are switched on (see the text for further details).

and κ is the inverse Debye length defined for a 1:1 electrolyte by

$$\kappa^2 = 2e^2 C N_A / \epsilon_r \epsilon_0 kT, \tag{6}$$

where e is the charge on the electron, N_A is Avogadro's number, and C is the ionic strength. For van der Waals attraction $U_A(r)$, we use the unretarded form[29]

$$U_A(r) = -(A_H/12)\{[4a^2/(r^2-4a^2)] + (2a/r)^2 + 2\ln[1-(2a/r)^2]\}, \tag{7}$$

where A_H is the effective Hamaker constant for the particles and the medium. For an isolated spherical particle of density ρ_1 in a Newtonian fluid medium of density ρ_0, the settling speed is given by

$$v = 2a^2(\rho_1 - \rho_0)gF_g/9\eta, \tag{8}$$

where η is the viscosity of the medium, and $F_g = 1$ for normal gravity ($g = 9.81\ \mathrm{m\ s^{-2}}$). The strength of the sedimenting force in relation to the fluctuating Brownian force is expressed by the Péclet number

$$Pe = av/D_0 = 4\pi F_g(\rho_1 - \rho_0)ga^4/3kT. \tag{9}$$

Equation (9) shows that the effect of Brownian motion is rapidly overwhelmed by the sedimenting field as particle radius increases.

III. DETAILS OF SEDIMENTATION AND DEPOSITION MODELS

In addition to the Brownian dynamics model with hydrodynamic interactions, two other simple models were studied to provide a link with earlier work; we call these the "pure ballistic" and "pure Brownian" models. All the models have certain features in common. Spherical particles of radius 0.25 μm move one at a time in a simulation cell of dimensions $10\,\mu\mathrm{m} \times 10\,\mu\mathrm{m} \times \infty$. The cell is periodic in the x and y directions, and the sedimenting field acts in the z direction. When a sedimenting particle comes into contact with another particle in the sediment (or gets within a small "coagulating" distance of another particle in the sediment), it is deemed to stick irreversibly. Alternatively, if it reaches the solid base of the cell ($z = 0$), it sticks there—this is the dominant mechanism early on in a simulation run. In either case, once particle-cluster aggregation has occurred, another particle is introduced at a random position in the x–y plane at a location some way above the highest point of the existing sediment, and the sedimentation of the new particle is simulated. The run is stopped when 2500 particles have been accumulated in the sediment at the bottom of the simulation cell.

The three different deposition models have the following individual characteristics:

(i) *Pure ballistic model*: In this simple model, each sedimenting sphere follows a linear trajectory in the z direction and does not interact with other particles in any way until contact.

(ii) *Pure Brownian model*: This differs from (i) only in respect of the addition of a purely random Brownian component to the dynamics through the use of Eq. (2) with $\mathsf{D}_{ij} = D_0 1$. No hydrodynamic or DLVO interactions are included. For efficient running, however, computational details differ substantially from the pure ballistic case. A sphere is released far above the sediment and is moved rapidly and linearly until within $\sim 8a$ of the nearest particle in the sediment. At this point Brownian motion is "switched on" with a timestep of 50 μs. When the moving sphere gets within $5a$ of the nearest sediment particle, Δt is reduced to 20 μs until aggregation occurs. (These schemes are reversed if, due to Brownian motion, the sphere moves away from the sediment).

(iii) *Brownian dynamics model*: Here, colloidal and hydrodynamic interactions are included as described in Sec. II. Figure 1 shows the reaction box for this type of simulation run. As with model (ii), the initial trajectory is linear until the sphere gets within $8a$ of the nearest particle in the sediment. At this point Brownian motion is switched on ($\mathsf{D}_{ij} = D_0 1$) with a timestep of 50 μs, and hydrodynamic interactions are included at the level of the Rotne–Prager tensor in the term $\mathsf{D}^{\circ}_{ij}\mathbf{F}_j$ in Eq. (1) with contributions to $\mathbf{F}_j$ only from the external field at this stage. When the sedimenting sphere gets within $5a$ of the deposit, Δt is reduced to 20 μs, and at this separation DLVO forces start to become significant and are therefore included. Also, stochastic weightings are now calculated from Eq. (2) using the full Rotne–Prager diffusion tensor at the level of nearest-neighbor hydrodynamics (i.e., including the hydrodynamic interaction between the sedimenting sphere and its nearest neighbor in the sediment). Aggregation is deemed to have occurred when $U \leqslant -10\ \mathrm{kT}$. We take $(\rho_1 - \rho_0) = 100\ \mathrm{kg\ m^{-3}}$ as in earlier work.[8]

The three coagulating DLVO colloidal potentials investigated here are plotted in Fig. 2. The parameter values in Eqs. (4)–(7) are set as follows: $\psi_0 = 20$ mV, $\epsilon_r = 80$, $T = 300$ K, $A_H = 1.94 \times 10^{-19}$ J. The three potentials of mean force differ only in their values of ionic strength C.

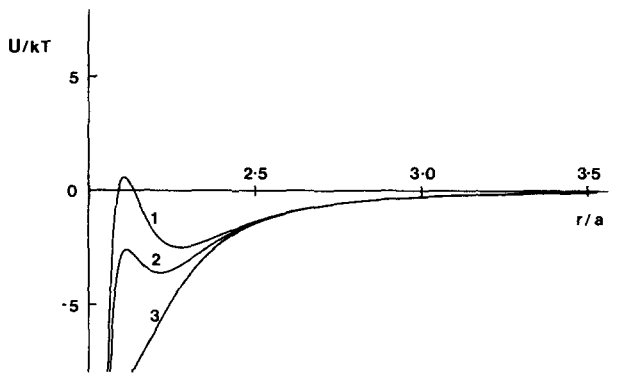

FIG. 2. DLVO potentials of mean force between pairs of colloidal particles. The energy $U(r)$ in units of kT is plotted against the center-to-center separation r in units of the particle radius a: 1, $C = 0.3$ mol m^{-3}; 2, $C = 0.375$ mol m^{-3}; 3, $C = 0.6$ mol m^{-3}.

Potential 1 ($C = 0.3$ mol m^{-3}) has a significant repulsive barrier (primary maximum) and attractive well (secondary minimum); potential 3 ($C = 0.6$ mol m^{-3}) is entirely attractive; and potential 2 ($C = 0.375$ mol m^{-3}) has a shape intermediate between the two. The presence of a potential energy barrier in $U(r)$ reduces the simulated coagulation rate[8,9,27] and therefore allows more time for structural reorganization prior to the irreversible aggregation step. The timesteps referred to above are for simulations at a field strength $F_g = 500$ ($Pe = 1.93$); in simulation runs at $F_g = 1500$ and 5000 ($Pe = 5.79$ and 19.3) the timesteps are reduced to 25 μs for $8a \geq r > 5a$ and 5 μs for $r \leq 5a$. At the largest Péclet number studied sedimentation is the predominant influence on particle motion, whereas at the lowest Péclet number Brownian motion is very important but the field strength is still sufficiently strong to ensure that sediment accumulation is reasonably efficient.

IV. RESULTS AND DISCUSSION

The gross effects of colloidal forces, hydrodynamic interactions, and field strength on sediment structure are indicated in Table I which shows the mean particle volume fraction in sediments produced under a variety of simulation conditions. The values refer to volume fractions in the middle region of the sediment between a plane at $z = 8a$ and another parallel plane at a distance $8a$ below the highest point of the deposit. Averages were taken over 5 simulation runs in each case, except at the higher field strengths where only three runs were carried out. The estimated error in volume fraction is ± 0.01.

TABLE I. Sediment density obtained under various simulation conditions (BD = Brownian dynamics with hydrodynamic interactions).

Model	Volume fraction
Pure ballistic	0.14
Pure Brownian	0.09
BD (potential 1, 500 g)	0.12
BD (potential 2, 500 g)	0.09_5
BD (potential 3, 500 g)	0.09
BD (potential 1, 1500 g)	0.20
BD (potential 1, 5000 g)	0.33

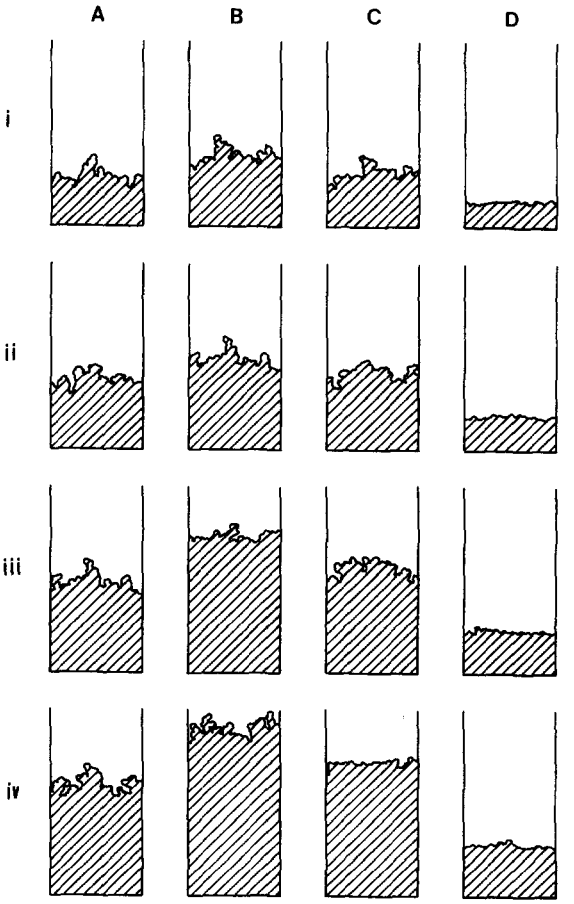

FIG. 3. Pictures of evolving sediment profiles are viewed from the y direction after deposition of (i) 1000 particles, (ii) 1500 particles, (iii) 2000 particles, and (iv) 2500 particles: (A) pure ballistic model; (B) pure Brownian model; (C) Brownian dynamics with $F_g = 500$ and potential 1; (D) Brownian dynamics with $F_g = 500$ and potential 1. Small holes in the sediment structures are not shown.

Some qualitative differences between evolving sediment profiles under different conditions are illustrated in Fig. 3. Snapshots of projections through the unit cell in the x–z plane are shown after deposition of 1000, 1500, 2000, and 2500 particles. There is a striking difference between the comparative smoothness of the surface of the sediment formed at $F_g = 5000$ and the ragged surface profiles of the three lower density sediments. Most dendritic in structure is the sediment produced by the pure Brownian model, which is in keeping with the previously reported findings of Meakin.[11,13]

In discussing the results, let us first consider the different models under conditions of low field strength ($F_g = 500$). Table I shows that the pure ballistic model gives sediments that are ~60% more dense than those produced by the pure Brownian model. This is qualitatively in line with lattice simulations[30,31] which have shown that aggregates formed ballistically are space filling on a long-length scale, whereas Brownian diffusion-limited aggregates are much looser due to screening effects. The density difference between sediments formed by pure ballistic and pure Brownian models is clearly seen in Fig. 4, which shows all the

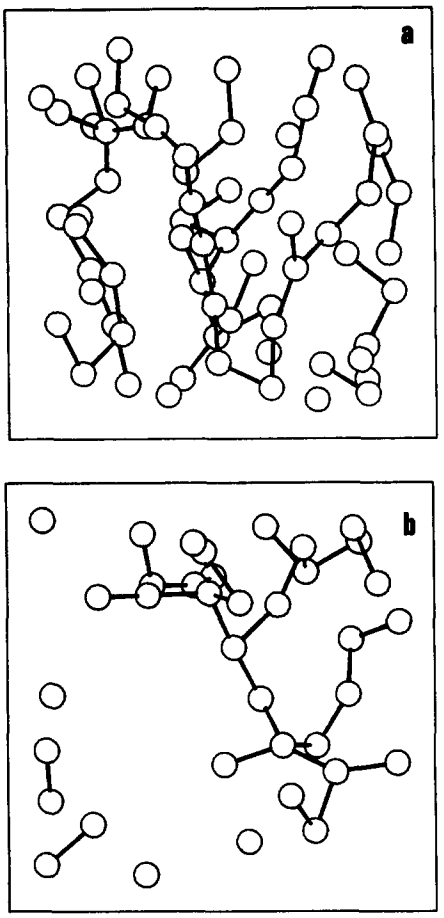

FIG. 4. Three-dimensional representations of particles within a $12a \times 12a \times 12a$ box in the middle of sediments generated with (a) pure ballistic model and (b) pure Brownian model. The box is viewed from the y direction, and the sedimenting force acts downwards as drawn. For clarity the spheres are represented as circles of smaller radius than a, with "bonds" between pairs of particles denoting points of direct contact produced by coagulation. Apparently "loose" particles are connected to other sediment particles outside the box. Note the large hole in the structure from the pure Brownian model.

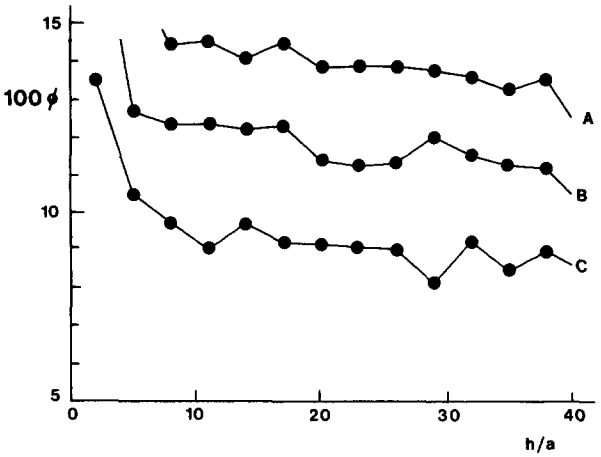

FIG. 5. Density profiles for sediments simulated at $F_g = 500$. The particle volume fraction ϕ is plotted against the height h above the base of the cell: (A) pure ballistic model; (B) Brownian dynamics with potential 1; (C) pure Brownian model. Each point corresponds to the mean density in a horizontal layer of thickness $3a$. Data from Brownian dynamics runs with potentials 2 and 3 are very similar to C.

particles and particle–particle contacts in cubes of size $12a$ in the centers of the sediments. The ballistic sediment appears partially clustered, while the Brownian sediment is highly dendritic. In the process of sedimentation, where the external field is constant in a single direction, the ballistic trajectories have a uniquely defined direction, and so for geometrical reasons they cannot truly be space filling, although there is much less screening than with the Brownian trajectories which give the moving particles a high effective cross section (a high walk dimensionality in fractal terminology[32]). As one would expect for low density fractal-type structures, the volume fraction is not absolutely independent of height even in the middle of the sediment. However, the particle density profiles plotted in Fig. 5 are sufficiently constant to enable clear differences to be discerned between the various models, and to enable reasonably reliable sediment volume fractions to be extracted. In principle, of course, the limiting density is only reached at infinite time. In practice, however, we believe that the numbers reported in Table I correspond to limiting volume fractions within the statistical uncertainty, based on observations of simulated density profiles as a function of the number of deposited particles.

In lattice-based simulations, Meakin found[11] a volume fraction of ~ 0.04 for Brownian sediments and ~ 0.33 for ballistic sediments. Even allowing for the increase in volume fraction inherent in going from sphere deposition to cube deposition, our volume fractions are substantially different. This is probably mainly due to the transition from square lattice to off-lattice simulations, which is likely to be particularly significant in a system where the driving field (sedimentation) is parallel to the lattice planes. In the case of ballistic trajectories, it appears as if a nonlattice model gives greater screening and therefore less dense sediments. In the nonlattice Brownian simulation, there is the possibility of an infinite number of trajectories in an infinite number of possible directions, and this tends to make the holes in the growing sediment more accessible to mobile intruding particles than with the square-lattice simulation. In addition, our density profile for the pure Brownian case (see Fig. 5) is much less dependent on height than that of Meakin.[11] This probably represents the fact that we are in a different scaling regime from that of Meakin, whose reaction box had a surface area 25 times greater than that used here.

We now move on to the Brownian dynamics simulations including colloidal interparticle forces and hydrodynamic interactions. From Table I and Fig. 5, we see that DLVO potential 1 gives a sediment of density intermediate between those for the pure ballistic and pure Brownian models. Potentials 2 and 3 give the same density profiles as the pure Brownian case within the statistical uncertainty. At these field strengths ($Pe \sim 2$) and with these colloidal potentials, the presence of hydrodynamic interactions makes very little difference to the simulated sediment structure. But the nature of the colloidal forces is more important. When the primary maximum is small (potential 2) or nonexistent (potential 3), the van der Waals attraction gives rise to rapid coagulation.[8,9] With a larger primary maximum, and more importantly, a deeper secondary minimum (potential 1),

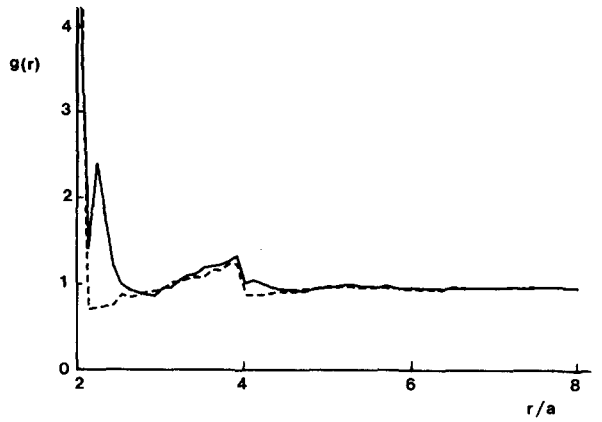

FIG. 6. Distribution function $g(r)$ of pairs of particles separated by distance r in simulated sediments: —, potential 1, $F_g = 500$; ---, potential 3, $F_g = 500$.

the moving particle will on average diffuse for some time in the vicinity of another particle in the sediment before aggregating irreversibly. In this latter case, the moving particle has access to more energetically favorable configurations before it finally jumps over the primary maximum, driven by Brownian motion and (to a lesser extent under these conditions) the external field. Moving from potential 3 to potential 1 is to some extent equivalent to reducing the sticking probability in the lattice-based simulations: In both cases there is an increase in the local particle density.

Figure 6 shows the pair distribution function $g(r)$ of particles in the deposits generated with potentials 1 and 3. The curves are normalized in the usual way such that $g(r) = 1$ corresponds to a random distribution. The plots were constructed by including in the averaging all pairs for which at least one of the particles was positioned between $z = 8a$ and a distance $8a$ below the top of the sediment. End effects at top and bottom are apparent if a larger slab of sediment is considered. The curves in Fig. 6 show similar features to radial distribution functions generated in two-dimensional cluster–cluster aggregation with the same DLVO potentials.[9] The $g(r)$ for potential 1 has a peak at $r \approx 2.3a$ which is completely absent with potential 3 (as it is for potential 2 and for the pure Brownian model). The peak at $r \approx 2.3a$ is associated with a high probability of pairs of nonbonded particles being found at a separation corresponding to the bottom of the secondary minimum. Here we have an example of the way in which the average colloidal structure just before coagulation influences the short-range structure of the coagulum. The small peak in $g(r)$ near $r = 4a$ represents the relatively high probability of finding three particles in a nearly linear configuration in these stringy sediment structures. The small but sharp drop in $g(r)$ just beyond $r = 4a$ is a real effect, due to the comparatively low probability of nonbonded pairs being separated by $r = 4a + \delta$ relative to $r = 4a - \delta$.

Turning now to the data generated with the higher sedimenting forces, the most immediately apparent result is the large increase in sediment volume fraction with increasing field strength. Figure 7 shows sediment portions from Brownian dynamics simulations with DLVO potential 1 at

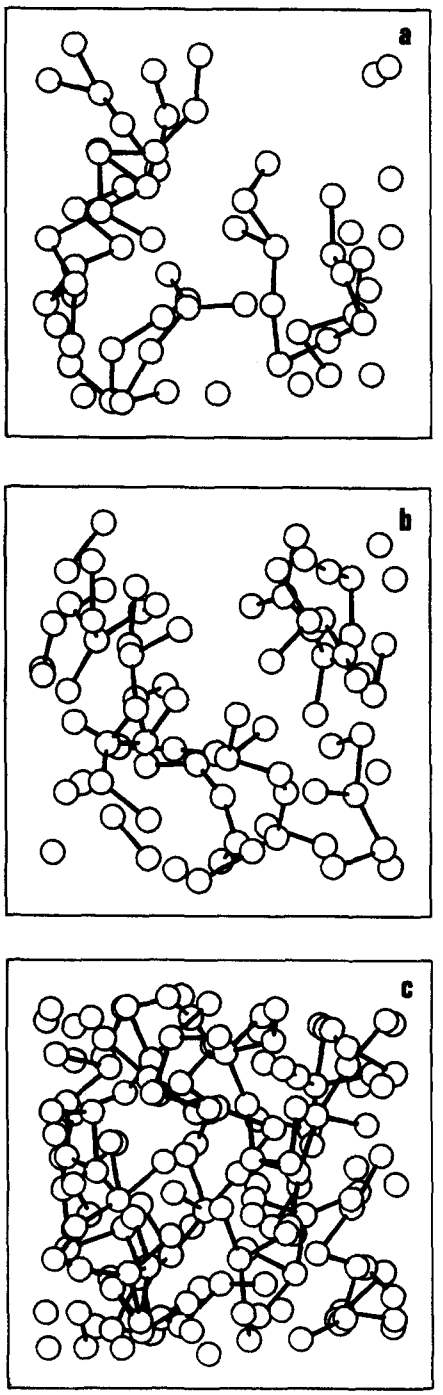

FIG. 7. Exploded views of portions of sediments simulated with potential 1 at three field strengths: (a) $F_g = 500$; (b) $F_g = 1500$; (c) $F_g = 5000$. Details as for Fig. 4.

$F_g = 500$, 1500, and 5000. The series of pictures shows how the sediment changes from a low-density stringy structure at low Péclet number to a compact, clustered structure at high Péclet number. The role of the hydrodynamic interactions becomes important at high field strengths, as the Brownian component of the dynamics becomes virtually swamped by the sedimentation component. The time scale for the moving particle to slip past a stationary particle in the sediment becomes larger than the time scale for Brownian coagulation over the potential energy barrier. The effect is similar to that already observed for an isolated pair of DLVO particles of

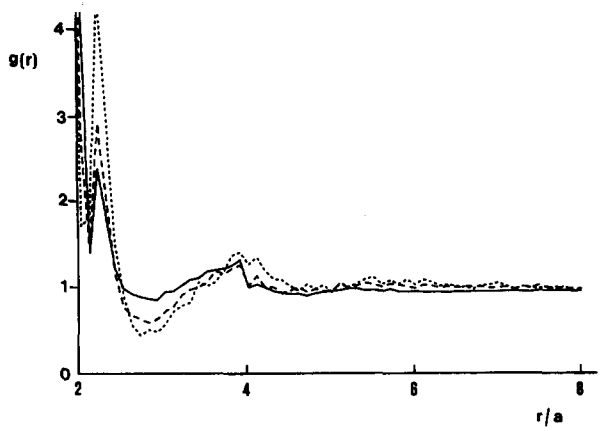

FIG. 8. Distribution function $g(r)$ of pairs of particles separated by distance r in sediments simulated with potential 1 at three field strengths: —, $F_g = 500$; – – –, $F_g = 1500$; ---, $F_g = 5000$.

different sizes.[33] The net result is a dense sediment with additional particles tending to fill up the holes in the existing structure. The limiting case of this behavior occurs when colloidal attractive forces and Brownian motion are both completely absent: The structure approaches that of randomly packed hard spheres (volume fraction 0.64).

Figure 8 shows the dependence on field strength of the pair distribution function $g(r)$ in sediments produced from particles interacting with potential 1. We notice how, as the sediment volume fraction increases, the structure of the amorphous sediment gets more and more like that of a simple liquid.[34] That is, the $g(r)$ curves become smoother with larger peaks and troughs, and the steep drop near $r = 2.4a$ becomes particularly prominent. This is not really too surprising: One would intuitively expect there to be a close relationship between the structure of a dense aggregated state and the prior liquid-like structure in the system before aggregation. With the simulations at $F_g = 5000$, we notice a slight increase in sediment density ($\sim 1\%$–2%) as the last 1000 particles are added which is not found at the lower field strengths. This may be due to a slow continuing "settling down" period following the rather arbitrary initialization stage.

Quantitative differences between the close-ranged structures of the various simulated sediments are given in Table II. Values of $g(r)$ at intervals of $0.1a$ are tabulated for $2a \leq r < 5a$. (For impenetrable spheres, the value is zero for $r < 2a$.) The statistical error in $g(r)$ is estimated to be at the 2%–3% level, and so the difference in structural results for potentials 2 and 3 at $F_g = 500$ is seen to lie only just outside the computational uncertainty. We note, however, that the close-ranged structure of the sediment generated by the pure Brownian model is rather different from that for potentials 2 or 3, even though the overall sediment densities are essentially the same (see Table I). At present there is very little pub-

TABLE II. Values of pair distribution function $g(r)$ for various separations r in simulated sediments (F_g = field strength relative to normal gravity; a = particle radius; BAL = pure ballistic model; BRO = pure Brownian model; POT1 = potential 1; POT2 = potential 2; POT3 = potential 3).

r/a	BAL	BRO	$F_g = 500$ POT1	$F_g = 500$ POT2	$F_g = 500$ POT3	$F_g = 1500$ POT1	$F_g = 5000$ POT1
2.0	10.49	10.27	10.13	11.64	11.27	9.71	7.72
2.1	2.42	3.18	4.48	5.03	5.13	2.94	1.79
2.2	0.65	0.65	1.47	1.02	0.73	1.46	1.93
2.3	0.74	0.72	2.49	0.95	0.75	3.05	4.61
2.4	0.77	0.82	1.89	0.89	0.77	2.15	3.14
2.5	0.79	0.85	1.27	0.78	0.78	1.20	1.56
2.6	0.84	0.89	1.03	0.81	0.90	0.80	0.94
2.7	0.85	0.92	0.96	0.81	0.87	0.71	0.59
2.8	0.90	1.00	0.93	0.86	0.90	0.67	0.47
2.9	0.92	0.97	0.91	0.95	0.94	0.62	0.54
3.0	0.96	1.05	0.89	0.95	0.95	0.67	0.51
3.1	0.96	1.06	0.99	1.02	0.98	0.76	0.61
3.2	1.00	1.04	1.00	1.03	1.05	0.82	0.76
3.3	1.02	1.11	1.07	1.12	1.05	0.95	0.82
3.4	1.11	1.11	1.13	1.12	1.09	1.01	0.86
3.5	1.11	1.11	1.15	1.14	1.11	1.04	1.10
3.6	1.14	1.15	1.23	1.17	1.11	1.10	1.06
3.7	1.18	1.18	1.25	1.20	1.20	1.24	1.10
3.8	1.27	1.22	1.27	1.21	1.20	1.20	1.23
3.9	1.31	1.24	1.31	1.23	1.27	1.27	1.42
4.0	1.34	1.27	1.37	1.33	1.28	1.31	1.46
4.1	0.94	0.95	1.04	0.93	0.90	1.06	1.32
4.2	0.98	0.96	1.08	0.89	0.91	1.18	1.40
4.3	0.98	0.99	1.04	0.91	0.90	1.04	1.24
4.4	0.99	0.98	0.99	0.96	0.92	1.05	1.14
4.5	1.00	1.02	0.97	0.94	0.95	0.97	1.13
4.6	1.04	1.03	0.96	0.96	0.94	1.01	1.06
4.7	1.05	1.03	0.97	0.98	0.94	1.04	1.00
4.8	1.05	1.01	0.94	1.00	0.98	0.99	1.08
4.9	1.06	1.04	0.97	1.00	0.98	1.02	1.02

lished data with which to compare the results in Table II, although recent work on random porous materials suggests[35] that it may be possible to get detailed structural information on coagulated gels from x-ray scattering experiments. On the theoretical side, it is pertinent to mention that $g(r)$ for the simulated sediment structure has some features similar to those found[36] with reversibly aggregated systems of sticky particles: A high probability of particles being in contact ($r = 2a$), a peak corresponding to the linear three-particle arrangement ($r = 4a$), and a sharp drop afterwards ($r > 4a$) except at high field strengths. On the other hand, whereas the sticky particles have a tendency to arrange themselves in semicrystalline ordered aggregates, there is no evidence for such local lattice-like structures in the gel-like sediments simulated here.

Our simulation results suggest that sediment structure is affected by the nature of short-ranged hydrodynamic interactions prior to coagulation, but is relatively unaffected by long-ranged hydrodynamic interactions. At the point when hydrodynamic interactions are switched on in the Brownian dynamics runs (see Fig. 1), the difference between D_{ij} and D_0 in Eq. (3) can be as much as 15%, but the effect of this is just to slow down the relative Brownian motion. When the cutoff distance was reduced from $8a$ to $6a$ in preliminary test simulations, no differences in sediment structure were detectable within the statistical error.

V. CONCLUSIONS

We have presented a simulation model of sediment formation by interacting colloidal particles which is a considerable improvement in realism over previous lattice-based models. The inclusion of hydrodynamic interactions and colloidal forces between aggregating particles leads to structures that are not only quantitatively, but qualitatively, different from those obtained with simple Brownian or ballistic models. Since even small changes in gel structure and volume fraction can lead to large changes in mechanical properties, the simulations reported here should provide useful information for the development of theories which aim to relate rheological behavior to colloidal interactions.

There are two main improvements which could be made to the model to make it even more realistic. Firstly, we have included hydrodynamic interactions only at the level of nearest-neighbor Rotne–Prager expressions. While we believe that this approximation contains the essential physics, it is possible that the fine details of sediment structure may be affected by multibody hydrodynamic effects, and it would therefore be interesting to include such effects in future work. Secondly, our sedimentation model is equivalent experimentally to a colloid at infinite dilution, since we do not allow particles to aggregate, or even to interact, before sticking to the sediment. It would be interesting to extend the present work to the case of a sedimenting nondilute system, i.e., a simulation in which a certain amount of ClCl aggregation occurs during the settling process.

ACKNOWLEDGMENTS

G. C. A. acknowledges receipt of a Studentship from the Ministry of Agriculture, Fisheries, and Food (U.K.). E. D. acknowledges support from SERC (U.K.).

[1]T. A. Witten and L. M. Sander, Phys. Rev. Lett. **47**, 1400 (1981).
[2]See, for instance, *Kinetics of Aggregation and Gelation*, edited by F. Family and D. P. Landau (Elsevier, Amsterdam, 1984); and *On Growth and Form: Fractal and Non-Fractal Patterns in Physics*, edited by H. E. Stanley and N. Ostrowsky (Martinus Nijhoff, Dordrecht, 1986).
[3]A. J. Hurd and D. W. Schaefer, Phys. Rev. Lett. **54**, 1048 (1985).
[4]D. A. Weitz, J. S. Huang, M. Y. Lin, and J. Sung, Phys. Rev. Lett. **54**, 1416 (1985).
[5]G. Y. Onoda, Phys. Rev. Lett. **55**, 226 (1985).
[6]A. J. Armstrong, R. C. Mocklet, and W. J. O'Sullivan, J. Phys. A **19**, L123 (1986).
[7]E. Dickinson, Chem. Soc. Rev. **14**, 421 (1985).
[8]J. Bacon, E. Dickinson, and R. Parker, Faraday Discuss. Chem. Soc. **76**, 165 (1983).
[9]G. C. Ansell and E. Dickinson, Chem. Phys. Lett. **122**, 594 (1985).
[10]J. P. Ryckaert, G. Ciccotti, and H. J. C. Berendsen, J. Comput. Phys. **23**, 327 (1977); S. A. Allison and J. A. McCammon, Biopolymers **23**, 167 (1984).
[11]P. Meakin, Phys. Rev. A **27**, 2616 (1983).
[12]Z. Racz and T. Vicsek, Phys. Rev. Lett. **51**, 2382 (1983).
[13]P. Meakin, J. Colloid Interface Soc. **104**, 282 (1985).
[14]R. F. Voss and M. Tomkiewicz, J. Electrochem. Soc. **132**, 371 (1985).
[15]P. Turq, F. Lantelme, and H. L. Friedman, J. Chem. Phys. **66**, 3039 (1977).
[16]D. L. Ermak and H. Buckholz, J. Comput. Phys. **35**, 169 (1980).
[17]W. F. van Gunsteren, H. J. C. Berendsen, and J. A. C. Rullmann, Mol. Phys. **44**, 69 (1981).
[18]F. J. Vesely, Mol. Phys. **53**, 505 (1984).
[19]D. L. Ermak and J. A. McCammon, J. Chem. Phys. **69**, 1352 (1978).
[20]E. Dickinson, S. A. Allison, and J. A. McCammon, J. Chem. Soc. Faraday Trans. 2 **81**, 591 (1985).
[21]G. K. Batchelor, J. Fluid Mech. **74**, 1 (1976).
[22]B. U. Felderhof, Physica A **89**, 373 (1977); R. Schmitz and B. U. Felderhof, *ibid.* **116**, 163 (1982).
[23]R. B. Jones and G. S. Burfield, Physica A **133**, 152 (1985).
[24]P. Mazur and W. van Saarloos, Physica A **115**, 21 (1982).
[25]J. Rotne and S. Prager, J. Chem. Phys. **50**, 4831 (1969).
[26]J. Garcia de la Torre and V. A. Bloomfield, Q. Rev. Biophys. **14**, 81 (1981).
[27]J. Bacon, E. Dickinson, R. Parker, N. Anastasiou, and M. Lal, J. Chem. Soc. Faraday Trans. 2 **79**, 91 (1983).
[28]E. J. W. Verwey and J. Th. G. Overbeek, *Theory of Stability of Lyophobic Colloids* (Elsevier, Amsterdam, 1948).
[29]J. Mahanty and B. W. Ninham, *Dispersion Forces* (Academic, London, 1976).
[30]P. Meakin, J. Colloid Interface Sci. **96**, 415 (1983).
[31]D. Bensimon, E. Domany, and A. Aharony, Phys. Rev. Lett. **51**, 1394 (1983).
[32]B. B. Mandelbrot, *The Fractal Geometry of Nature* (Freeman, San Francisco, 1982).
[33]E. Dickinson and R. Parker, J. Colloid Interface Sci. **97**, 220 (1984).
[34]J. A. Barker and D. Henderson, Rev. Mod. Phys. **48**, 587 (1976).
[35]D. W. Schaefer and K. D. Keefer, Phys. Rev. Lett. **56**, 2199 (1986).
[36]N. A. Seaton and E. D. Glandt, J. Chem. Phys. **84**, 4595 (1986).